Environmental Science & Technology

pubs.acs.org/est

Article

Persistent Influence of Wildfire Emissions in the Western United States and Characteristics of Aged Biomass Burning Organic Aerosols under Clean Air Conditions

Ryan Farley, Noah Bernays, Daniel A. Jaffe, Damien Ketcherside, Lu Hu, Shan Zhou, Sonya Collier, and Qi Zhang*

Cite This: *Environ. Sci. Technol.* 2022, 56, 3645−3657

Read Online

ACCESS | Metrics & More | Article Recommendations | Supporting Information

ABSTRACT: Wildfire-influenced air masses under regional background conditions were characterized at the Mt. Bachelor Observatory (~2800 m a.s.l.) in summer 2019 to provide a better understanding of the aging of biomass burning organic aerosols (BBOAs) and their impacts on the remote troposphere in the western United States. Submicron aerosol (PM_1) concentrations were low (average ± 1σ = 2.2 ± 1.9 $\mu g\ sm^{-3}$), but oxidized BBOAs (average O/C = 0.84) were constantly detected throughout the study. The BBOA correlated well with black carbon, furfural, and acetonitrile and comprised above 50% of PM_1 during plume events when the peak PM_1 concentration reached 18.0 $\mu g\ sm^{-3}$. Wildfire plumes with estimated transport times varying from ~10 h to >10 days were identified. The plumes showed ΔOA/ΔCO values ranging from 0.038 to 0.122 ppb ppb^{-1} with a significant negative relation to plume age, indicating BBOA loss relative to CO during long-range transport. Additionally, increases of average O/C and aerosol sizes were seen in more aged plumes. The mass-based size mode was approximately 700 nm (D_{va}) in the most oxidized plume that likely originated in Siberia, suggesting aqueous-phase processing during transport. This work highlights the widespread impacts that wildfire emissions have on aerosol concentration and properties, and thus climate, in the western United States.

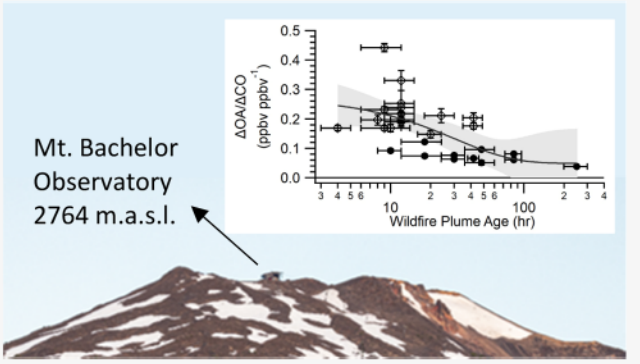

KEYWORDS: *aerosol mass spectrometry, soot-particle aerosol mass spectrometer (SP-AMS), submicrometer aerosols (PM_1), biomass burning organic aerosols (BBOAs), atmospheric aging, long-range transport*

1. INTRODUCTION

Biomass burning (BB) is a major source of atmospheric aerosols and significantly impacts global climate, public health, and regional air quality.[1−3] Depending on the physical properties and chemical composition of the aerosols, they can scatter or absorb solar radiation, act as cloud condensation nuclei, and alter cloud albedo.[4−7] BB is a large source of both primary organic aerosols (POA) and volatile organic compounds (VOCs) that can act as precursors for secondary organic aerosols (SOA).[8−10] BB is also a large source of brown carbon (BrC), an aerosol component that is able to absorb sunlight in the visible wavelengths and positively influence global climate forcing.[11−13]

Wildfires are a highly variable and "uncontrollable" source of BB emissions that cause haze in both pristine areas and urban centers.[3,14] In the western United States, wildfires are becoming increasingly prevalent, and their emissions have been tied to elevated regional $PM_{2.5}$ concentrations and high pollution episodes that violated National Ambient Air Quality Standards (NAAQS).[3,15−20] Additionally, studies are continuing to show that wildfire plumes are able to influence aerosol loading and atmospheric chemistry up to thousands of kilometers from the source.[21−24] Furthermore, OA that has undergone atmospheric processing has been found to be more detrimental to human health.[25,26] A deeper understanding of the chemical and optical properties of wildfire emissions and the evolution of BB aerosols in the atmosphere will help constrain atmospheric chemical transport models and global climate models.[4,27−29]

Biomass burning organic aerosols (BBOAs) can have a wide range of volatility, with the volatility generally decreasing with increased atmospheric processing.[18,30,31] The oxidation of VOCs and intermediate volatility organic compounds

Received: October 27, 2021
Revised: February 17, 2022
Accepted: February 18, 2022
Published: March 1, 2022

(IVOCs) emitted from BB has been seen to form low-volatility products, which can increase SOA production and the atmospheric lifetime of the aerosols.[32−34] The exact properties of BBOA are highly dependent on burn conditions, fuel type, and the magnitude of atmospheric processing.[9,18,35−40] While many previous studies have investigated the composition of fresh fire emissions in laboratory and ambient conditions, as well as the transformation of BBOA in fire plumes over the course of the first hours of atmospheric aging,[40,41] only a few have investigated highly processed wildfire emissions at remote locations such as islands,[42,43] high-altitude locations,[44−46] and the remote troposphere.[24,47] These studies have found that long-range transport of BB emissions can cause episodic increases of aerosol concentrations and that multiple days of aging may significantly influence ambient BB aerosol characteristics. However, it remains poorly understood how wildfire emissions and atmospheric aging processes affect the chemical composition and physical properties of background aerosols in pristine environments, and what impacts these have on climate.

In the present study, we provide an overview of the physical and chemical properties of aerosol particles and trace gases studied using a suite of real-time instruments at the Mt. Bachelor Observatory (MBO), a remote, high-altitude site in the American Pacific Northwest (PNW) during the summer of 2019. MBO has been operated as an atmospheric chemistry observatory since 2004,[27] and due to its remote location and minimal anthropogenic influence, it is an ideal site for measurements of wildfire plumes ranging from locally emitted to long-range transport events from Alaska and Asia.[17,18,27,48,49] During this study, hereafter named MBO19, we show that regionally transported BBOA is an important component of submicrometer aerosols (PM_1) even during periods of relatively low fire activity and aerosol loading. In addition, we utilize the variety of BB plume sources to understand how aerosol properties change as a function of physical and photochemical age.

2. METHODS

2.1. Sampling Site. An intensive measurement campaign was conducted at the MBO, located at the summit of Mt. Bachelor (43.981°N 121.691°W, 2764 m a.s.l.) from August 1 to September 10, 2019. Mt. Bachelor is an isolated volcanic peak approximately 31 km east of the city of Bend, Oregon (population 80,000). Few wildfires were active upwind of MBO during the sampling period, although there were fires throughout western North America (Figure S1). In comparison, heavy wildfire plumes originating in Northern California and Southern Oregon were frequently sampled during the summer 2013 Biomass Burning Observation Period (BBOP) campaign at MBO (Figures S1 and S2).[18,19,35]

Boundary layer dynamics play an important role in the diurnal variation of aerosol composition at MBO. During daytime, upslope air can bring modified boundary layer (MBL) air masses to the sampling site, while at night, the site is influenced by free tropospheric (FT) air masses.[27,50] These different regimes can be differentiated based on ambient water vapor concentrations with values greater than 5.23 and 4.60 g kg^{-1} corresponding to MBL conditions during August and September, respectively.[27]

2.2. Real-Time Measurements. Size-resolved aerosol composition and volatility were studied at 2 min time resolution using a soot-particle aerosol mass spectrometer (SP-AMS; Aerodyne Research, Inc.) downstream of a custom-built, automated thermodenuder (TD, Figure S3). The SP-AMS and its use in studying wildfire smokes are described in detail elsewhere.[40,51,52] Briefly, the instrument operates by focusing aerosols through an aerodynamic lens with a size cutoff of 1 μm aerodynamic diameter (PM_1). Particles are then sized prior to colliding with a 600 °C resistively heated tungsten vaporizer. The resulting gaseous molecules are ionized by 70 eV electron impact and are detected using a high-resolution time-of-flight mass spectrometer.[53,54] In this study, the SP-AMS was operated only in the lower mass resolution ($m/\Delta m$ = 2500) and higher sensitivity "V-Mode" for an increased signal-to-noise (S/N) ratio, allowing the bulk ensemble mass spectra for nonrefractory (NR) PM_1 to be calculated.[54] This includes the quantification of organics, the ammonium salts of sulfate, nitrate, and chloride. The SP-AMS also allows for the simultaneous quantification of refractory black carbon (rBC) using an intracavity laser vaporizer.[51,52] A thermodenuder based on the design described in Fierz et al. was installed upstream of the SP-AMS to quantify aerosol volatility.[55] Additional information regarding SP-AMS operation and thermodenuder temperature settings is given in SI Section 1.2 and Figures S3−S5.

Information on additional real-time instrumentation deployed during this study is provided in SI Section 1.2.3. Briefly, speciated VOC measurements were made every 1 min with a proton transfer reaction time-of-flight mass spectrometer (PTR-ToF-MS 4000, Ionicon Analytik, Austria), with the mass resolution up to $m/\Delta m$ 4000.[56] The PTR-ToF-MS background was checked every hour. During the campaign, it was calibrated every 2 days by the dynamic dilution and subsequent addition of 25 distinct VOCs including furfural and acetonitrile from gas standard mixtures.[57] A scanning mobility particle sizer (SMPS) consisted of a TSI 3082 electrostatic classifier with a TSI 3776 water-based condensation particle counter collected number distribution at a 5 min time resolution between 14 and 615 nm. In addition, other data used in this study include CO (Picarro G2302 cavity ring-down spectroscopy) and submicrometer aerosol scattering coefficients (σ_{sp}) at wavelengths 450, 550, and 700 nm (TSI Model 3563 integrating nephelometer). CO and σ_{sp} data are reported in 5 min averages. The σ_{sp} values were corrected for drift and scattering truncation according to the scheme laid out by Anderson and Ogren.[58] Additional calibration details are provided in Briggs et al.[17] In this study, we focused on σ_{550nm}, which correlated well ($r^2 > 0.96$) with both σ_{700nm} and σ_{450nm}.

2.3. SP-AMS Data Analysis and Positive Matrix Factorization Analysis. SP-AMS results were analyzed with the SQUIRREL (v. 1.53A) and PIKA (v. 1.23A) software packages in Igor Pro (v. 8 Wavemetrics, Lake Oswego, OR). All mass concentrations were determined using the high-resolution mass spectral (HRMS) data and are reported in STP conditions (273.15 K, 101325 Pa), notated with "μg sm^{-3}". Additional details regarding the SP-AMS ionization efficiency calibration and treatment of gas-phase interference are given in the SI Section 1.2.1. The SP-AMS limit of detection (LOD) was calculated as 3 times the standard deviation during an extremely clean period when the average ($\pm 1\sigma$) SMPS mass concentration was 0.013 ($\pm$0.017) μg sm^{-3}. The LOD was 139, 18, 18, 9, 25, and 53 ng m^{-3} for organics, nitrate, sulfate, chloride, ammonium, and black carbon, respectively, for an averaging time of 2 min. These LOD values are higher than expected due to the decreased S/N caused by the installation of a radio frequency filter on the SP-

https://doi.org/10.1021/acs.est.1c07301
Environ. Sci. Technol. 2022, 56, 3645−3657

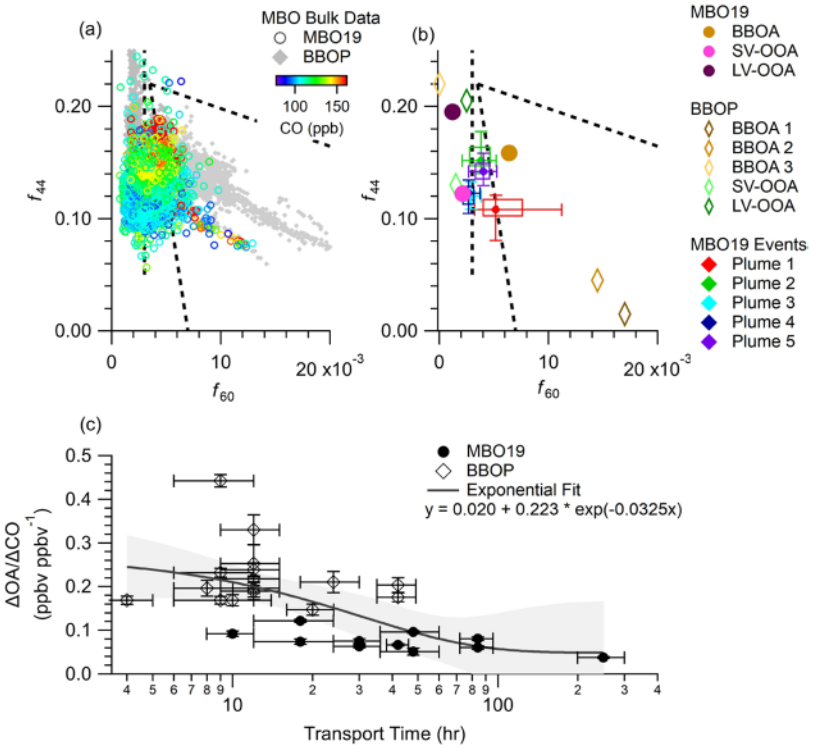

Figure 1. Overview of BBOA characteristics and the influences of atmospheric aging based on observations made during MBO19 and BBOP. Scatterplots of f_{44} and f_{60} for (a) bulk OA data and (b) OA factors resolved through PMF analysis of the SP-AMS data. (c) Changes in ΔOA/ΔCO with estimated transport times of wildfire plumes. The MBO19 data in (a) is colored by CO concentration. The dashed black lines in (a) and (b) represent the background f_{60} value of 0.3% and the boundaries set for ambient BBOA in Cubison et al. (2011). Data points with OA < 1 μg sm^{-3} were removed to reduce noise. The f_{44} and f_{60} values in the five wildfire plume events identified during MBO19 are indicted by the colored boxes in (b), with the box bounds representing the 25th and 75th percentiles, and the error bars representing the 10th and 90th percentiles. Points in (c) are the MBO19 wildfire plume events and BB plumes identified in Collier et al. (2016). The solid line in (c) is the best fit of all of the points with the gray area representing the 95th confidence interval. The fitting equation is provided in the legend of (c).

AMS to reduce signal interference from nearby equipment, including cell phone transmitters. The molar ratios of elements (O/C and H/C) for the bulk OA were calculated using the "Improved Ambient" method.[59]

Positive matrix factorization (PMF)[60] was used to decompose the SP-AMS HRMS data using the PMF evaluation tool (PET)[61] into a set of static factors and their time-dependent contributions. The association of individual factors with specific emission sources or atmospheric processes was examined through analyses of the spectra, temporal variation patterns, and comparison with external tracers.[62] The time series of organic ions, major inorganic ions, and TD data during both the laser on and laser off periods were included within the PMF analysis to decrease ambiguity in the solution space and provide insight into the volatility of each factor.[18,63] A detailed description of the preparation, analysis, and evaluation of PMF solutions is given in SI Section 1.3 and Figures S6–S8. The final PMF solution consists of a low-volatility oxygenated OA (LV-OOA), a semivolatile oxygenated OA (SV-OOA), and a BBOA.

3. RESULTS AND DISCUSSION

3.1. Aerosol Characteristics at MBO during Summer 2019. The concentrations of different aerosol components varied dynamically at MBO throughout the campaign (Figure S9). Generally, low PM_1 concentrations were seen during summer 2019, ranging from <0.14 to 18.0 μg sm^{-3} with an average (±1σ) of 2.22 (±1.86) μg sm^{-3}. Aerosol loading was on average dominated by organics (82.1%), followed by sulfate (11.3%), ammonium (4.1%), rBC (2.4%), and nitrate (2.0%) with chloride and potassium at or below LOD for most the campaign. The meteorology was typical for summer at a high-altitude site: the temperature ranged from −1.6 to 20.7 °C (average ± 1σ of 12.0 ± 4.5 °C) and RH varied from 7.4 to 100% (52 ± 23%). Although the weather was typically cool and dry, there were periods when MBO was in clouds and rain, which coincided with the lowest PM_1 concentrations.

MBO has been used extensively for trace gas and aerosol measurements since 2004, allowing for data comparisons with previous campaigns. Specifically, the results from 2019 are compared to the HR-AMS data collected at MBO during the BBOP in summer 2013, which is discussed in previous publications.[17−19,35,50] Substantially, higher PM_1 concentrations (up to 210 μg sm^{-3}) were sampled in 2013,[18] whereas the MBO19 measurements allow for detailed chemical characterization of discrete BB plumes that are significantly more aged and diluted than those sampled in 2013. The average PM_1 concentration during MBO19 is consistent with low loading periods observed during BBOP (NR-PM_1 = 2.8 ± 2.8 μg sm^{-3}), as well as other high-altitude, background sites around the world (3.8 ± 3.4 μg sm^{-3}).[50]

A commonly used HR-AMS tracer for BB is the signal at m/z 60 over the total OA signal, known as f_{60}.[37] In this study, over 95% of the signal at m/z 60 is from the $C_2H_4O_2^+$ ion (m/z = 60.021), a fragment primarily generated from anhydrous sugars (e.g., levoglucosan) during cellulous combustion.[64−66] For

https://doi.org/10.1021/acs.est.1c07301
Environ. Sci. Technol. 2022, 56, 3645−3657

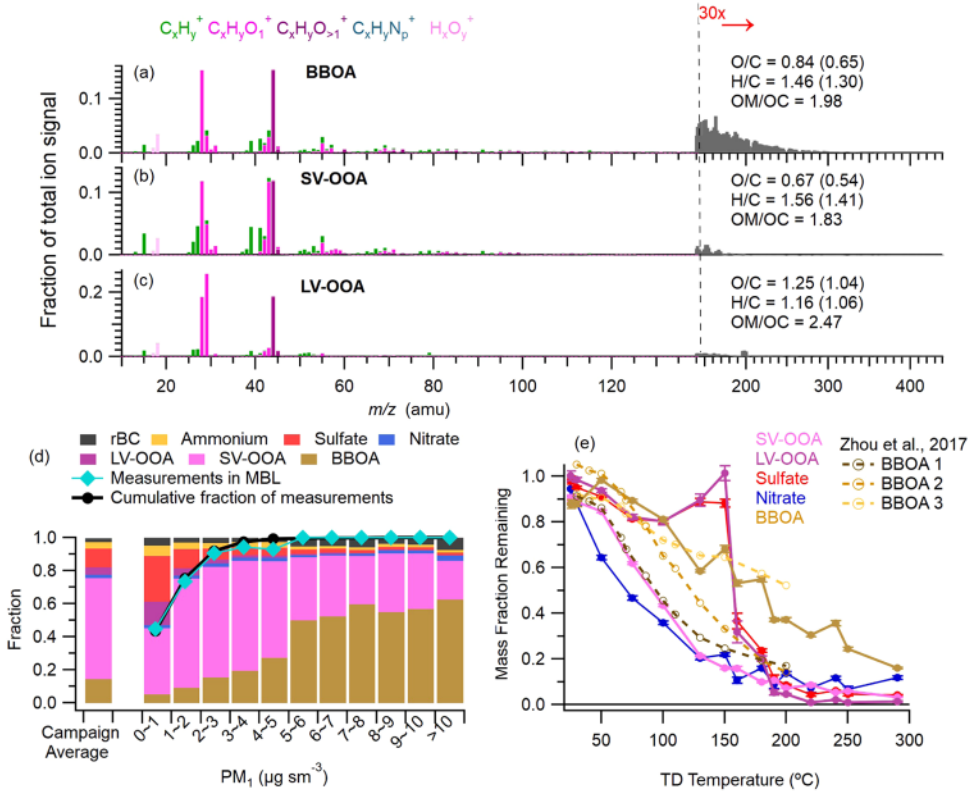

Figure 2. (a–c) Spectra of OA factors colored by ion family. HRMS ions are included for m/z < 140, and UMR ions for m/z > 140. "Improved Ambient" elemental ratios for each factor are denoted in the legend, with the "Aiken Ambient" value in parenthesis. (d) Fractional contribution of each species as a function of total PM_1 loading. (e) Volatility profiles of OA factors, sulfate, and nitrate. Error bars show the standard deviation of the calculated slope. BBOA factors derived in Zhou et al. 2017 are also included for reference in (e).

ambient OA, f_{60} < 0.3% generally represents no BB influence, while f_{60} > 1% represents prominent BB influence.[37] The campaign average of f_{60} was 0.29 ± 0.12% with events ranging up to 1.2% (Figures 1 and S12). The periods with elevated f_{60} also showed an increase in CO concentrations (up to 180 ppbv; Figure S9d), aerosol absorption and scattering (up to 6 and 70 Mm^{-1}, respectively, at 530 nm), and PM_1 (up to 18.0 $\mu g\ sm^{-3}$; Figure S9c). Additionally, there were elevated concentrations of rBC, acetonitrile, and furfural, all of which are BB tracers (Figure S9g).[39,67]

The relative abundance of anhydrous sugars in BB aerosols, as represented by f_{60}, has been found to decrease during atmospheric transport due to evaporation or decay of BB-POA and concurrent production of BB-SOA.[37] Indeed, the f_{60} values during this campaign are generally lower than in fresh wildfire plumes and are consistent with other aged BB plumes sampled during BBOP and at other remote locations.[18,35,37,68] Figure 1a,b compares the aerosol composition from MBO19 and BBOP in the f_{44}–f_{60} space. f_{44}, defined analogously to f_{60}, is dominated by the CO_2^+ fragment, correlates with bulk aerosol O/C ratio, and represents the level of oxidation of OA.[69] The f_{44}–f_{60} space is a common technique to investigate the effect of aging on the properties of BBOA with more aged/oxidized BBOA moving toward a lower f_{60} and a higher f_{44}.[37,70] During MBO19, OA spanned a wide range of f_{60} and f_{44} values, indicating the influence of BB as well as the presence of additional, non-BB sources at the site (Figures 1a and S11). CO is a well-known tracer for BB emissions. Although photo-oxidation of biogenic VOCs can be a significant source of CO in remote regions as well, the strong correlations between CO and BB tracers such as benzene, acetonitrile, and rBC suggest that the CO enhancements at MBO were largely due to BB influence. Figure 1a shows that elevated CO concentrations correspond with high f_{60} values as well as high f_{44} values, suggesting that BB is an important source of highly oxidized aerosols. Furthermore, the OA data from the MBO19 and BBOP campaigns overlapped in the f_{60}–f_{44} space (Figure 1a), suggesting similarities between the BBOA sources and atmospheric aging processes. However, BBOA in MBO19 was overall significantly more aged. In addition, Figure 1c shows a negative correlation between the enhancement ratio of OA relative to CO (ΔOA/ΔCO) in wildfire plumes and plume transport time, which highlights the impacts of atmospheric aging on BBOA characteristics (see detailed discussions in Section 3.4).

Nonsoil potassium salts (ns-K) have been identified as a tracer for BB in previous field studies.[66,71−73] SP-AMS is able to detect potassium through both surface ionization on the tungsten vaporizer[74] and laser vaporization of potassium salts internally mixed with rBC.[51,75] However, concentrations of K^+ were low and noisy throughout this campaign, which is consistent with previous studies finding minimal K^+ enhancements in wildfire plumes in this region of the PNW.[18,76] The reason for this lack of enhancement is unclear; however, previous studies have found K^+ emission dependent on fuel type.[77]

3.2. Organic Aerosol Sources at MBO and Biomass Burning Influences. To evaluate the influence of transported wildfire plumes on aerosol chemistry at MBO, PMF analysis was performed and resolved three meaningful factors. They

https://doi.org/10.1021/acs.est.1c07301
Environ. Sci. Technol. 2022, 56, 3645−3657

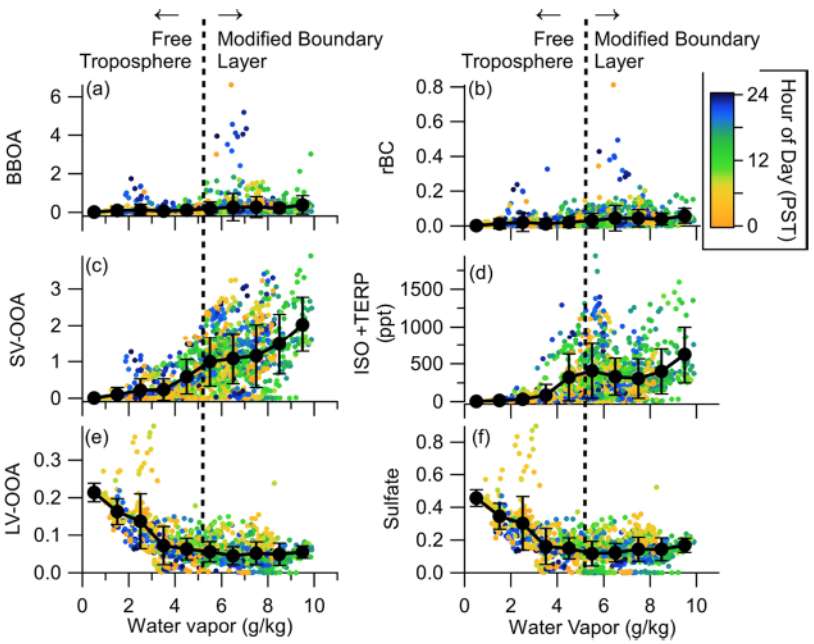

Figure 3. Concentration of species as a function of water vapor, colored by time of day. Solid black lines indicate the mean concentration within each water vapor mixing ratio bin, with errors bars indicating 1 standard deviation. The dashed line indicates the cutoff between the free troposphere and the modified boundary layer.[27] ISO+TERP shows the sum of isoprene and monoterpenes.

include a BBOA (O/C = 0.84, 18% of OA), a semivolatile oxygenated OA (SV-OOA) (O/C = 0.67, 76% of OA), and a low-volatility oxygenated OA (LV-OOA) (O/C = 1.25, 6% of OA). The factor mass spectra and volatility thermal profiles are shown in Figure 2, and the time series and diurnal profiles are shown in Figures S9 and S10. The time series of the BBOA factor correlated with rBC (r^2 = 0.52) and showed sporadic but large enhancements that are consistent with transported BB plumes (Figure S9e). The factor was moderately oxidized with an O/C of 0.84 and an f_{60} value of 0.64%. The MBO19 BBOA is situated between the moderately oxidized BBOA-2 and the highly oxidized BBOA-3 resolved during BBOP in the f_{44}–f_{60} space (Figures 1b and S10). The volatility profile of the MBO19 BBOA also falls between those of BBOA-2 and BBOA-3 (Figure 2e). These results highlight the fact that the oxidized BBOA observed at MBO contains extremely low-volatility species, e.g., 16% of the MBO19 BBOA mass was found to remain in the particle phase at TD temperature as high as 280 °C.

The variation of BBOA concentration correlated poorly with ambient water vapor, signifying that there was wildfire influence on aerosol composition within both the MBL and the FT (Figure 3). BB sources are almost exclusively located within the MBL, but large wildfires are able to inject aerosols into the FT, where the rate of deposition decreases and long-range transport of aerosols is facilitated.[23] This suggests that BBOA sampled within the FT is likely more heavily processed. In addition, since fires dominated by flaming combustion have larger plume injection heights and are more likely to penetrate the FT[78] plumes that have undergone long-range transport may be more likely to have been emitted by fires with high modified combustion efficiency (MCE) characteristic of flaming combustion.

The majority of the OA mass seen during MBO19 (76%) was contributed by the moderately oxidized SV-OOA factor (O/C = 0.67). There was a strong association of high concentrations of SV-OOA with higher water vapor values, occurring when MBO resided within the MBL (Figure 3) and the diurnal trends of the SV-OOA concentration and water vapor are similar (Figure S10b). Based on the correlation with gas-phase oxidation products such as methanol (r^2 = 0.82), methyl ethyl ketone (r^2 = 0.75), and formic acid (r^2 = 0.73), as well as significant contribution from $C_xH_y^+$ fragments in the HRMS (37% of the OA signal) and a high $C_2H_3O^+$ to CO_2^+ ratio of 0.99, this factor is likely primarily composed of biogenic SOA.[79,80] The increased concentration of SV-OOA between 11:00 and 20:00 likely represents an upslope flow of BL-influenced air that was enriched with fresh SOA produced through daytime photochemical processes of regional biogenic VOCs. Finally, the LV-OOA factor was highly oxidized (O/C = 1.25) with a significant contribution from CO_2^+ and CHO^+ ions in the HRMS (Figure 2c). This factor represents a highly oxidized, regional background aerosol and accounts for 6% of OA during MBO19. Additional details of the PMF solutions are described in SI Section 1.3.2.

The composition of PM_1 varied across the range of total PM_1 concentrations (Figure 2d). At very low PM_1 loadings (<1 $\mu g\ m^{-3}$), sulfate and LV-OOA together made up 41% of the PM_1 mass, with BBOA contributing only 5%, although there were periods with sulfate contributing up to 80% of total PM_1. Higher LV-OOA and sulfate concentrations were mostly seen at low water vapor values, primarily at night, when FT air masses were sampled (Figure 3). This is an indication that sulfate aerosols and highly oxidized OA were enhanced in the regional FT, a finding that is consistent with previous observations at MBO.[50] As the PM_1 loading increased, the fractional contribution from BBOA increased and contributions from sulfate and LV-OOA decreased. At $PM_1 > 5\ \mu g\ m^{-3}$, BBOA accounted for 50–62% of PM_1 mass (Figure 2d). These results highlight the important influences that wildfire emissions have on aerosols in the remote region of PNW, even under relatively clean air conditions.

3.3. Case Studies on Aged Wildfire Plumes at MBO.

The location of MBO gives us a unique opportunity to sample

https://doi.org/10.1021/acs.est.1c07301
Environ. Sci. Technol. 2022, 56, 3645−3657

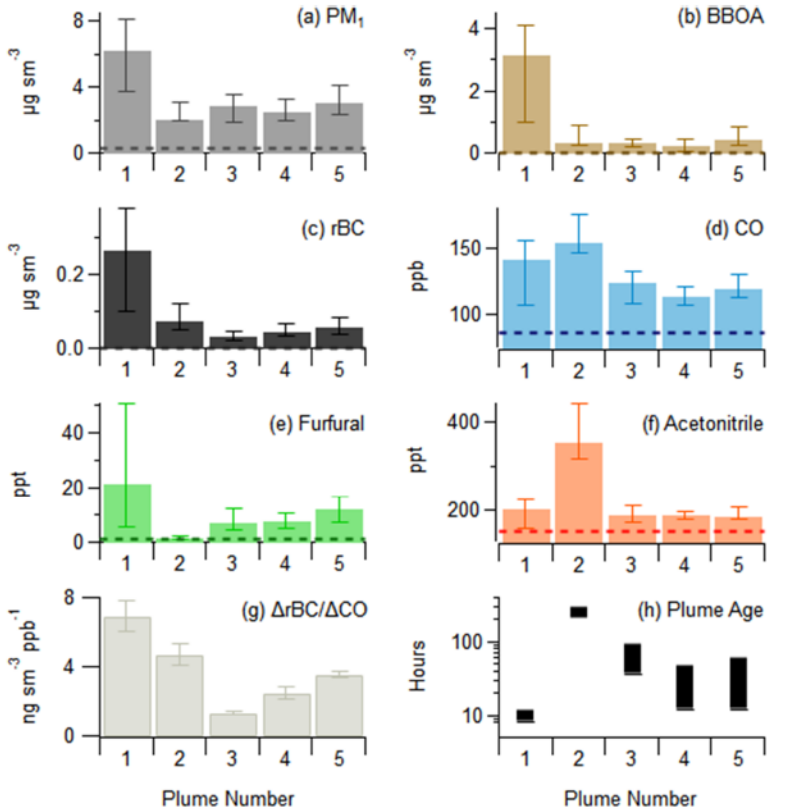

Plume Number	Duration (hr)	Probable Source Location	Approximate Distance to Source (km)
1	8	Milepost 97 fire 42.91, -123.27	180
2	14	Siberia	>4000
3	70	Northern California	250-350
4	19	Northern California	220-500
5	48	Northern California	150-540

Figure 4. (a–f) Median concentration of key particle and gas-phase species. Dashed lines represent the background concentrations of each species during the campaign, calculated as the 10th percentile of the species throughout the campaign. (g) rBC concentration normalized to CO. (h) Plume age estimated from HYSPLIT back trajectory. Whiskers indicate the 25th and 75th percentiles during each plume except for (g), where whiskers indicate 1σ of the orthogonal distance regression between the species. The transport time shown in Figure 5 spans between the closest and furthest fire detection that the plume passed over. The table shows a summary of the plume durations and likely sources of each plume event.

BB influenced air masses that had undergone substantial atmospheric processing and provides a glimpse into how atmospheric processing may influence the properties of aged BBOA. During this campaign, five distinct BB plume events (see shaded regions in Figure S9) were identified in a similar fashion as previous studies at MBO.[81] Specifically, plume events were defined as time periods satisfying the following conditions (1) CO > 110 ppb and σ_{550nm} > 20 Mm^{-1} and (2) r^2 between CO and PM$_1$ > 0.6. Overall, the plume periods showed increased PM$_1$ concentrations, dominated by OA, and elevated BBOA and rBC concentrations (Figure 4). The average HRMS of the bulk OA for each plume event is shown in Figure S16, and additional details are included in Figure S17.

Plume event 1 showed the highest PM$_1$ loadings with an average of 5.8 ± 3.1 μg sm^{-3} and the BBOA factor making up 52% of the total mass (Figure 4). HYSPLIT back trajectories show the sampled air mass passing over the Milepost 97 fire (42.913, −123.268) approximately 10 h prior to reaching MBO (Figure S18). This makes it a useful example for regionally emitted BBOA that has undergone relatively limited atmospheric processing. Indeed, this period appears to contain reasonably fresh BBOA with the f_{60} reaching 1.25% and $f_{>100mz}$ reaching 14.7%. The average HRMS during this period showed a high contribution from the $C_xH_y^+$ family, lower f_{44} and O/C of 0.45 (Figure S16). In contrast, plume event 2 showed significantly more oxidized aerosols (O/C = 0.69), a smaller f_{60} (0.50%), and a lower $f_{>100mz}$ (10.4%). It was characterized by extremely low water vapor mixing ratio (3.52 ± 0.99 g kg^{-1}) and was the only plume that was sampled within the FT. Back trajectory analysis of this event indicates that it was transported from a series of large fires in Siberia (Figure S19). Plume 2 also showed enhancement of sulfate and LV-OOA compared to the other plumes, which is consistent with highly aged aerosols transported within the FT (Figure S17). Events 3–5 represent BB plumes originating from active wildfires in Northern California with transport times estimated at 12–96 h (Figures S19–S21). Events 3 and 4 show f_{60} values of 0.30% and 0.25, respectively, close to the background f_{60} values (0.3 ± 0.06%) seen for ambient OA,[37] likely due to mixing with fresh,

https://doi.org/10.1021/acs.est.1c07301
Environ. Sci. Technol. 2022, 56, 3645−3657

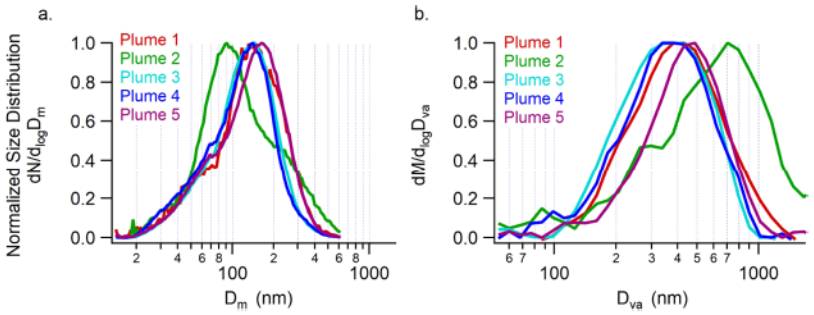

Figure 5. (a) Number-based size distribution of PM_1 measured by SMPS and (b) mass-based size distribution of organic aerosols measured by SP-AMS. Distributions are averaged for the duration of each plume.

biogenic SOA. Indeed, the OA of events 3 and 4 are significantly less oxidized than the BBOA-3 factor observed during BBOP, which also has f_{60} < 0.3% (O/C = 0.58 and 0.57, respectively, vs O/C = 1.06 for BBOA-3). Despite these characteristics, events 3 and 4 show enhancements of all other BB tracer species, confirming the influence from BB emissions (Figure 4). The OA within plume event 5 also showed characteristics of aged BBOA, with an O/C of 0.59 and an f_{60} of 0.39%.

The influence of plume processing on the concentration of gas-phase species is complex and shows significant variation between events. While both CO and acetonitrile were enhanced considerably during all of the plume periods, furfural was elevated only in less aged plumes (Figure 4e,f). This is because CO and acetonitrile are fairly inert in the atmosphere with a lifetime longer than 1 month,[82,83] whereas furfural reacts quickly with hydroxyl and nitrate radicals in wildfire plumes, thus may show lower enhancement in aged emissions. Indeed, as displayed in Figure 4e,h, the average enhancement of furfural concentration in individual events anticorrelates with plume age. The very low furfural concentration in plume 2 is consistent with the long-range transport and extensive atmospheric aging of the smoke originated from Siberia. Acetonitrile had the highest concentrations in event 2 and the smaller enhancements above the background within the other plume events may be due to either an elevated background concentration throughout the PNW due to the long lifetime or differing combustion conditions and fuel types at the different fires.[84,85]

The enhancement of rBC relative to the enhancement of CO (ΔrBC/ΔCO) can be used as an indicator of the combustion efficiency of the BB source with increased ΔrBC/ΔCO occurring during flaming combustion.[38,86,87] During each plume event, rBC showed moderate correlations with CO (r^2 ranging from 0.25 to 0.58) and the ΔrBC/ΔCO values were consistent with previous measurements of fresh and transported BB emissions.[86,88] The highest ΔrBC/ΔCO were measured during plume events 1 and 2, suggesting that these fires had more influence from flaming conditions. However, it is also possible that ΔrBC/ΔCO decreased during transport by two different pathways. First, rBC may be removed via deposition during long-range transport. This is most relevant to plume event 2 due to the possibility of wet deposition and cloud processing. Second, mixing of the BB plumes with CO produced from the oxidation of biogenic VOCs may enhance the background CO concentration. This could explain the lower values seen in plume events 3 and 4, which were most influenced by biogenic sources.

The size distributions during each plume event (Figures 5 and S23) can also provide insight into the processing history of the aerosols. Laboratory studies show that the mass-weighted size distributions of fresh BB aerosols are typically small (D_{va} < 100 nm) but quickly grow through condensation and coagulation over the course of aging.[89,90] In addition, at urban locations with intense residential wood burning, the mass-based size distribution of BBOA was found to be broad, presenting a smaller mode peaking between 150 and 200 nm and a larger mode peaking between 400 and 500 nm.[91,92] Plume events 1 and 5 both showed single modes, peaking at 400 and 500 nm, respectively, which is consistent with aged BBOA. This highlights the rapid growth of aerosols during the atmospheric transport of BB plumes. Event 2 also showed a single mode, but it peaks at 700 nm, suggesting more pronounced aqueous-phase processing during transport. This is also consistent with previous studies at MBO that have found BB plumes transported from Siberia have a larger size mode.[93] Interestingly, event 2 shows the smallest number-based size mode at 90 nm (Figure 5a). It is likely that this mode represents free tropospheric sulfate aerosol formed through new particle formation, a process that has been previously recorded at MBO.[50] Plume events 3 and 4 showed broad size distributions, between 250 and 500 nm, which can be explained by the mixing of BBOA with smaller biogenic SOA.

3.4. Evolution of Aerosol Properties in Aged Wildfire Plumes. The plume events identified during MBO19 allow for a quantitative analysis of the effect of prolonged aging on BB aerosol properties. Events 3−5 were further divided to optimize the correlations between OA and CO, as well as toluene and CO. For each event, the physical plume age was estimated from the HYSPLIT model and the photochemical age was determined based on the decay of toluene relative to CO (ΔToluene/ΔCO) or benzene (ΔToluene/ΔBenzene). The correlations between toluene and CO were strong during events 1, 3, and 4, with r^2 ranging from 0.79 to 0.95 (Figure S24). There was no enhancement of toluene during event 2 and therefore an r^2 of 0. Although the toluene signal was elevated during event 5, it had a negligible correlation with CO. The reason is unknown but could be due to the mixing of fresh and aged plumes or influence from anthropogenic emissions; therefore, event 5 was excluded from further analysis. Generally, ΔToluene/ΔCO, ΔToluene/ΔBenzene, and physical age were well correlated (Figure S26); however, ΔToluene/ΔCO showed a more consistent trend than ΔToluene/ΔBenzene and is discussed below as a proxy for photochemical age. Additional details regarding the ΔToluene/ΔCO calculation, the alternate use of ΔToluene/

https://doi.org/10.1021/acs.est.1c07301
Environ. Sci. Technol. 2022, 56, 3645−3657

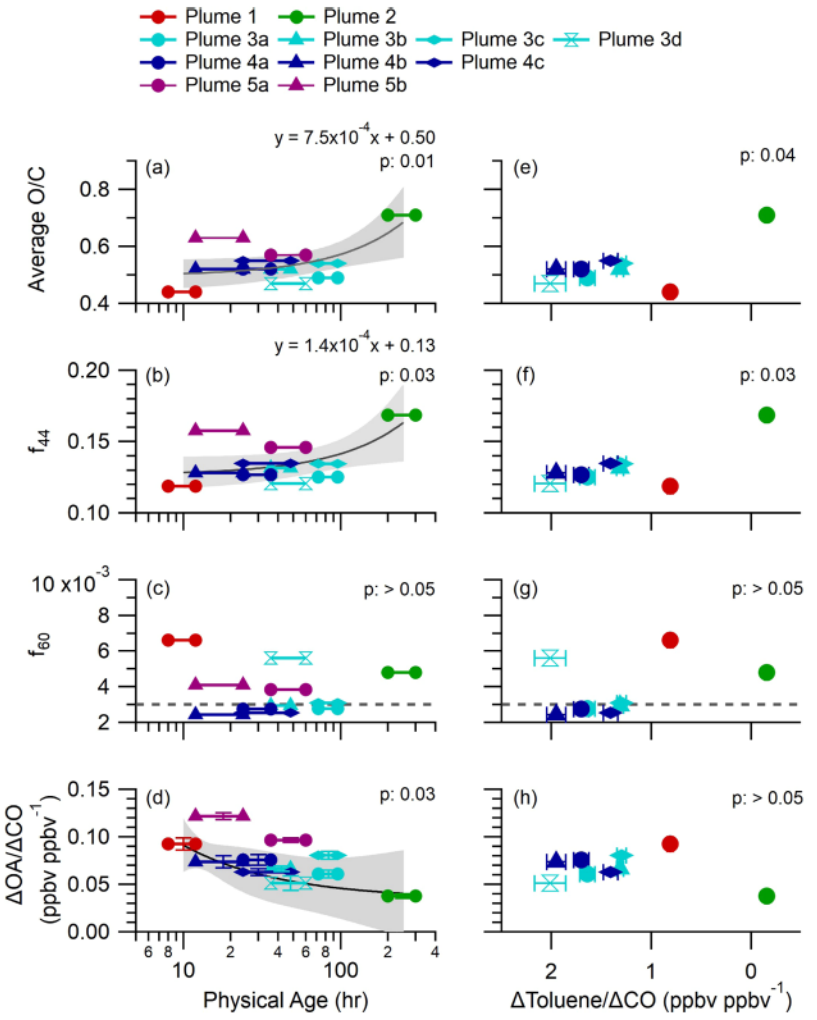

Figure 6. Relationships between aerosol properties and (a−d) physical age estimated from HYSPLIT back trajectories and (e−h) photochemical age calculated from ΔToluene/ΔCO. *p*-Value determined from two-tailed *t*-test. Note that plume 5 is not included in (e−h) due to lack of correlation between toluene and CO. Whiskers represent the error of the linear regression. ΔOA/ΔCO is calculated as a dimensionless ratio (ppbv ppbv^{-1}). Fit lines for the MBO19 data shown in (a), (b), and (d) are represented by the gray solid lines, with the gray area representing the 95th confidence interval.

ΔBenzene as a photochemical age metric, and comparison to literature values are described in SI Section 1.4.

Figure 6 shows the change in aerosol properties as a function of both the physical age and ΔToluene/ΔCO. There is a positive relation ($p < 0.05$) between both bulk OA O/C and f_{44} and plume physical age, indicating oxidation processes occurring during transport (Figure 6a,b). A negative relation is seen between f_{60} and physical age as well, after plume sections with f_{60} values below the 0.3% background value are excluded. This decreasing trend of f_{60} is consistent with the loss of anhydrous sugars during transport, which is also shown in Figure 1b. Here, the evolution of OA is seen within the f_{44}−f_{60} space as OA moves toward higher f_{44} values corresponding to increased plume processing (i.e., from event 1 to event 5 to event 2). Events 3 and 4 deviate from the trend line and are located more closely to the SV-OOA factor in the f_{44}−f_{60} space, likely due to influences by biogenic emissions (see discussions in Section 3.3).

Of particular interest is the change of the OA enhancement ratio relative to CO (ΔOA/ΔCO) with atmospheric aging (Figure 1c). ΔOA/ΔCO is independent of dilution but will change with either SOA production or OA losses through evaporation, deposition, and/or photodegradation reactions.[94] Some field and laboratory studies have found substantial SOA production during the aging of BB smoke,[70,95] while others have seen no enhancement[18,96] or a decrease in OA mass.[37,97] All of the plumes identified during MBO19 show good correlations between OA and CO ($r^2 > 0.70$) with enhancement ratios varying from 0.038 to 0.122 ppb ppb^{-1}. Significantly higher ΔOA/ΔCO (0.219 ± 0.067 ppb ppb^{-1}; calculated from Collier et al.[35]) were observed during BBOP for regionally transported, but less aged, wildfire plumes. The MBO values agree well with the ΔOA/ΔCO measured in wildfire plumes sampled during several aircraft campaigns compiled by Jolleys et al.,[94] where the flight-average values ranged from 0.019 ± 0.002 to 0.329 ± 0.006 ppb ppb^{-1} and the values were systematically higher in fresher plumes than in aged plumes.

A large range of ΔOA/ΔCO values, varying from 0.092 to 0.442 ppb ppb^{-1}, is seen at intermediate plume physical ages between 6 and 12 h at MBO (Figure 1c). This spread is likely due to differences in initial emission characteristics, such as the concentration of SOA precursors, burning condition, or fuel types.[35,98] However, at above 12 h, ΔOA/ΔCO shows a strong

https://doi.org/10.1021/acs.est.1c07301
Environ. Sci. Technol. 2022, 56, 3645−3657

negative trend ($p < 0.05$) with physical age (Figure 6d). This suggests either the continued evaporation of volatile BB-POA, OA loss via deposition, and heterogeneous oxidation or loss of BB-SOA via evaporation or fragmentation reactions. In addition, from this relationship, it appears that after 10−20 days of aging, ΔOA/ΔCO may begin to approach zero due to chemical destruction of BBOA. The extremely low ΔOA/ΔCO value seen in event 2 may also be affected by aerosol wet deposition during long-range transport. It is worth noting that this analysis represents a small population of BB plumes and more measurements of ΔOA/ΔCO at transport ages >1 day are needed to further probe this trend.

The ΔToluene/ΔCO was variable between the plumes, ranging from as high as 2 pptv ppbv^{-1} during plume 3 to 0 pptv ppbv^{-1} during plume 2, which is consistent with the loss of toluene through oxidation reactions (Figure 6). Overall, the trends seen between aerosol properties and ΔToluene/ΔCO agree well with the trends seen with physical age. However, due to the exclusion of plume 5 as discussed above, the relationships are less statistically robust. Furthermore, plume 1 appears to be an outlier; it displays a lower ΔToluene/ΔCO, indicating processing, despite a low O/C, short estimated physical age, and other signs of fresh BB. It is possible that this plume had a lower toluene emission ratio due to differences of MCE or fuel type in the fire. Despite this, ΔToluene/ΔCO appears to be a promising metric for quantifying photochemical age in aged BB plumes.

4. ATMOSPHERIC IMPLICATIONS

Our atmospheric measurement study in the summer of 2019 at MBO, a remote, high elevation site with minimal anthropogenic influence, allowed a unique chance to study aged aerosols with influence from wildfires. The results are relevant to the tropospheric background in western North America during wildfire season, which often spans most of summer and fall. The atmospheric conditions during this study were typical for a pristine remote location as the PM_1 concentration was very low (2.22 ± 1.86 μg sm^{-3}) and was dominated by organic species (81%). However, biomass burning evidently affected this site, as seen through increased concentrations of CO, rBC, acetonitrile, furans, and SP-AMS tracer ions for anhydrous sugars. Five mild wildfire plume events were observed and their transport times were estimated to vary from ∼10 h to >10 days. The OA in these aged wildfire plumes showed increasingly higher O/C ratio, larger size mode, and lower volatility with longer transport time and higher photochemical age. Additionally, a decrease of ΔOA/ΔCO as a function of transport time was seen, at a rate of approximately −0.022 ppb ppb^{-1} day^{-1}, suggesting a net loss of BBOA relative to CO during long-range transport caused by processes such as evaporation, photolysis, and deposition. Near-field measurements of BB plumes, however, often observed that ΔOA/ΔCO increased or remained constant during transport. These results yield important considerations for parameterizing the behavior of BBOA within global chemical transport and climate models over the course of multiple days, one of which is that it may not be appropriate to extrapolate changes in ΔOA/ΔCO based on near-field measurements out to multiple days.

PMF analysis of the SP-AMS mass spectra resolved an aged BBOA factor and two OOA factors representing SOA originated in the boundary layer and the free troposphere, respectively. The BBOA factor had a higher O/C (= 0.84) and a lower f_{60} (= 0.61%) compared to fresh BBOA factors but was consistent with the aged BBOA factors determined previously at MBO.[18] BBOA accounted for an average 18% of the OA mass during this study; however, there is evidence that the BBOA factor resolved by PMF in this study may have underestimated the contribution of BB to total OA and should be treated as a lower limit. As shown in Figure S15, there were time periods when the BBOA concentration approached 0 μg sm^{-3}, but rBC, CO, and furfural showed enhanced concentrations and strong correlations with total OA. Furthermore, the distribution of ion signals among the OA factors suggests that the SV-OOA factor was influenced by BB during low OA periods. For example, $C_2H_4O_2^+$ (m/z 60) and $C_3H_5O_2^+$ (m/z 73) are established BB tracers, but nearly 60% of their signals are attributed to the SV-OOA factor (Figure S14). Similar underestimations could occur during other field campaigns with low-concentration periods where data is analyzed by PMF. Finally, the volatility profile of the BBOA also highlights that aged BB emissions may represent an important source of low and extremely low-volatility organic compounds (LVOC and ELVOC) in remote areas. These results underscore the widespread influence of wildfires on aerosol properties and atmospheric chemistry in the western United States during summertime, which may have important implications on regional and global climate.

■ ASSOCIATED CONTENT

Supporting Information

The Supporting Information is available free of charge at https://pubs.acs.org/doi/10.1021/acs.est.1c07301.

Additional information on SP-AMS data collection and processing; brief description of colocated instrumentation; and details of PMF analysis and interpretation, as well as the calculation of back trajectories and photochemical age (PDF)

■ AUTHOR INFORMATION

Corresponding Author

Qi Zhang − *Department of Environmental Toxicology, University of California Davis, Davis, California 95616, United States; Agricultural and Environmental Chemistry Graduate Group, University of California Davis, Davis, California 95616, United States;* orcid.org/0000-0002-5203-8778; Phone: (530)-752-5779; Email: dkwzhang@ucdavis.edu

Authors

Ryan Farley − *Department of Environmental Toxicology, University of California Davis, Davis, California 95616, United States; Agricultural and Environmental Chemistry Graduate Group, University of California Davis, Davis, California 95616, United States*

Noah Bernays − *School of Science, Technology, Engineering, and Mathematics, University of Washington Bothell, Bothell, Washington 98011, United States*

Daniel A. Jaffe − *School of Science, Technology, Engineering, and Mathematics, University of Washington Bothell, Bothell, Washington 98011, United States;* orcid.org/0000-0003-1965-9051

Damien Ketcherside − *Department of Chemistry and Biochemistry, University of Montana, Missoula, Montana 59812, United States*

https://doi.org/10.1021/acs.est.1c07301
Environ. Sci. Technol. 2022, 56, 3645−3657

Lu Hu − *Department of Chemistry and Biochemistry, University of Montana, Missoula, Montana 59812, United States*

Shan Zhou − *Department of Environmental Toxicology, University of California Davis, Davis, California 95616, United States;* Present Address: Department of Civil and Environmental Engineering, Rice University, Houston, Texas 77005, United States; orcid.org/0000-0001-5031-1024

Sonya Collier − *Department of Environmental Toxicology, University of California Davis, Davis, California 95616, United States;* Present Address: California Air Resources Board, 1001 I Street, Sacramento, California 95814, United States

Complete contact information is available at: https://pubs.acs.org/10.1021/acs.est.1c07301

Notes

The authors declare no competing financial interest.

■ ACKNOWLEDGMENTS

This research was supported by the U.S. National Science Foundation (Grant #AGS-1829803 to UC Davis and 1650275 to U Montana), the U.S. Department of Energy's Atmospheric System Research Program (Grant #DE-SC0014620 and DE-SC0022140), and the California Agricultural Experiment Station (Project CA-D-ETX-2102-H). R.F. also acknowledges funding from the Jastro-Shields Research Award and the Matsumura Memorial Fellowship from the University of California at Davis. The authors thank Wade Permar, Ahsan Mozaffar, and Dr. Joel Thornton for their help during the field deployment. The Mt. Bachelor Observatory is supported by the National Science Foundation (grant #AGS-1447832) and the National Oceanic and Atmospheric Administration (contract #RA-133R-16-SE-0758).

■ REFERENCES

(1) IPCC. Summary for Policymakers. In *Climate Change 2014: Impacts, Adaptation, and Vulnerability. Part A: Global and Sectoral Aspects. Contribution of Working Group II to the Fifth Assessment Report of the Intergovernmental Panel on Climate Change*; IPCC, 2013.

(2) Pope, C. A.; Dockery, D. W. Health Effects of Fine Particulate Air Pollution: Lines That Connect. *J. Air Waste Manage. Assoc.* **2006**, *56*, 709−742.

(3) Jaffe, D. A.; O'Neill, S. M.; Larkin, N. K.; Holder, A. L.; Peterson, D. L.; Halofsky, J. E.; Rappold, A. G. Wildfire and Prescribed Burning Impacts on Air Quality in the United States. *J. Air Waste Manage. Assoc.* **2020**, *70*, 961−970.

(4) Shrivastava, M.; Cappa, C. D.; Fan, J.; Goldstein, A. H.; Guenther, A. B.; Jimenez, J. L.; Kuang, C.; Laskin, A.; Martin, S. T.; Ng, N. L.; Petaja, T.; Pierce, J. R.; Rasch, P. J.; Roldin, P.; Seinfeld, J. H.; Shilling, J.; Smith, J. N.; Thornton, J. A.; Volkamer, R.; Wang, J.; Worsnop, D. R.; Zaveri, R. A.; Zelenyuk, A.; Zhang, Q. Recent Advances in Understanding Secondary Organic Aerosol: Implications for Global Climate Forcing. *Rev. Geophys.* **2017**, *55*, 509−559.

(5) Quaas, J.; Ming, Y.; Menon, S.; Takemura, T.; Wang, M.; Penner, J. E.; Gettelman, A.; Lohmann, U.; Bellouin, N.; Boucher, O.; Sayer, A. M.; Thomas, G. E.; McComiskey, A.; Feingold, G.; Hoose, C.; Kristjnsson, J. E.; Liu, X.; Balkanski, Y.; Donner, L. J.; Ginoux, P. A.; Stier, P.; Grandey, B.; Feichter, J.; Sednev, I.; Bauer, S. E.; Koch, D.; Grainger, R. G.; Kirkevaring, A.; Iversen, T.; Seland, O.; Easter, R.; Ghan, S. J.; Rasch, P. J.; Morrison, H.; Lamarque, J. F.; Iacono, M. J.; Kinne, S.; Schulz, M. Aerosol Indirect Effects General Circulation Model Intercomparison and Evaluation with Satellite Data. *Atmos. Chem. Phys.* **2009**, *9*, 8697−8717.

(6) Twomey, S. Pollution and the Planetary Albedo. *Atmos. Environ.* **1974**, *8*, 1251−1256.

(7) Brown, H.; Liu, X.; Pokhrel, R.; Murphy, S.; Lu, Z.; Saleh, R.; Mielonen, T.; Kokkola, H.; Bergman, T.; Myhre, G.; Skeie, R. B.; Watson-paris, D.; Stier, P.; Johnson, B.; Bellouin, N.; Schulz, M.; Vakkari, V.; Beukes, J. P.; Van Zyl, P. G.; Liu, S.; Chand, D. Biomass Burning Aerosols in Most Climate Models Are Too Absorbing. *Nat. Commun.* **2021**, *12*, No. 277.

(8) Hallquist, M.; Wenger, J. C.; Baltensperger, U.; Rudich, Y.; Simpson, D.; Claeys, M.; Dommen, J.; Donahue, N. M.; George, C.; Goldstein, A. H.; Hamilton, J. F.; Herrmann, H.; Hoffmann, T.; Iinuma, Y.; Jang, M.; Jenkin, M. E.; Jimenez, J. L.; Kiendler-Scharr, A.; Maenhaut, W.; McFiggans, G.; Mentel, T. F.; Monod, A.; Prévôt, A. S. H.; Seinfeld, J. H.; Surratt, J. D.; Szmigielski, R.; Wildt, J. The Formation, Properties and Impact of Secondary Organic Aerosol: Current and Emerging Issues. *Atmos. Chem. Phys.* **2009**, *9*, 5155−5236.

(9) Gilman, J. B.; Lerner, B. M.; Kuster, W. C.; Goldan, P. D.; Warneke, C.; Veres, P. R.; Roberts, J. M.; De Gouw, J. A.; Burling, I. R.; Yokelson, R. J. Biomass Burning Emissions and Potential Air Quality Impacts of Volatile Organic Compounds and Other Trace Gases from Fuels Common in the US. *Atmos. Chem. Phys.* **2015**, *15*, 13915−13938.

(10) Jen, C. N.; Hatch, L. E.; Selimovic, V.; Yokelson, R. J.; Weber, R.; Fernandez, A. E.; Kreisberg, N. M.; Barsanti, K. C.; Goldstein, A. H. Speciated and Total Emission Factors of Particulate Organics from Burning Western US Wildland Fuels and Their Dependence on Combustion Efficiency. *Atmos. Chem. Phys.* **2019**, *19*, 1013−1026.

(11) Andreae, M. O.; Gelencsér, A. Black Carbon or Brown Carbon? The Nature of Light-Absorbing Carbonaceous Aerosols. *Atmos. Chem. Phys.* **2006**, *6*, 3131−3148.

(12) Bond, T. C.; Bergstrom, R. W. Light Absorption by Carbonaceous Particles: An Investigative Review. *Aerosol Sci. Technol.* **2006**, *40*, 27−67.

(13) Adler, G.; Wagner, N. L.; Lamb, K. D.; Manfred, K. M.; Schwarz, J. P.; Franchin, A.; Middlebrook, A. M.; Washenfelder, R. A.; Womack, C. C.; Yokelson, R. J.; Murphy, D. M. Evidence in Biomass Burning Smoke for a Light-Absorbing Aerosol with Properties Intermediate between Brown and Black Carbon. *Aerosol Sci. Technol.* **2019**, *53*, 976−989.

(14) Jaffe, D.; Hafner, W.; Chand, D.; Westerling, A.; Spracklen, D. Interannual Variations in PM2.5 Due to Wildfires in the Western United States. *Environ. Sci. Technol.* **2008**, *42*, 2812−2818.

(15) Westerling, A. L.; Hidalgo, H. G.; Cayan, D. R.; Swetnam, T. W. Warming and Earlier Spring Increase Western U.S. Forest Wildfire Activity. *Science* **2006**, *313*, 940−943.

(16) McClure, C. D.; Jaffe, D. A. US Particulate Matter Air Quality Improves except in Wildfire-Prone Areas. *Proc. Natl. Acad. Sci. U.S.A.* **2018**, *115*, 7901−7906.

(17) Briggs, N. L.; Jaffe, D. A.; Gao, H.; Hee, J. R.; Baylon, P. M.; Zhang, Q.; Zhou, S.; Collier, S. C.; Sampson, P. D.; Cary, R. A. Particulate Matter, Ozone, and Nitrogen Species in Aged Wildfire Plumes Observed at the Mount Bachelor Observatory. *Aerosol Air Qual. Res.* **2016**, *16*, 3075−3087.

(18) Zhou, S.; Collier, S.; Jaffe, D. A.; Briggs, N. L.; Hee, J.; Iii, A. J. S.; Kleinman, L.; Onasch, T. B.; Zhang, Q. Regional Influence of Wildfires on Aerosol Chemistry in the Western US and Insights into Atmospheric Aging of Biomass Burning Organic Aerosol. *Atmos. Chem. Phys.* **2017**, *17*, 2477−2493.

(19) Zhang, Q.; Zhou, S.; Collier, S.; Jaffe, D.; Onasch, T.; Shilling, J.; Kleinman, L.; Sedlacek, A. Understanding Composition, Formation, and Aging of Organic Aerosols in Wildfire Emissions via Combined Mountain Top and Airborne Measurements. In *Multiphase Environmental Chemistry in the Atmosphere*; ACS Symposium Series; American Chemical Society, 2018; Vol. *1299*, pp 363−385.

(20) Sedlacek, A. J.; Buseck, P. R.; Adachi, K.; Onasch, T. B.; Springston, S. R.; Kleinman, L. Formation and Evolution of Tar Balls from Northwestern US Wildfires. *Atmos. Chem. Phys.* **2018**, *18*, 11289−11301.

(21) Hung, W. T.; Lu, C. H. S.; Shrestha, B.; Lin, H. C.; Lin, C. A.; Grogan, D.; Hong, J.; Ahmadov, R.; James, E.; Joseph, E. The Impacts of Transported Wildfire Smoke Aerosols on Surface Air Quality in New York State: A Case Study in Summer 2018. *Atmos. Environ.* **2020**, *227*, No. 117415.
(22) Teakles, A. D.; So, R.; Ainslie, B.; Nissen, R.; Schiller, C.; Vingarzan, R.; McKendry, I.; Marie Macdonald, A.; Jaffe, A. D.; Bertram, K. A.; Strawbridge, B. K.; Richard Leaitch, W.; Hanna, S.; Toom, D.; Baik, J.; Huang, L. Impacts of the July 2012 Siberian Fire Plume on Air Quality in the Pacific Northwest. *Atmos. Chem. Phys.* **2017**, *17*, 2593−2611.
(23) Baars, H.; Ansmann, A.; Ohneiser, K.; Haarig, M.; Engelmann, R.; Althausen, D.; Hanssen, I.; Gausa, M.; Pietruczuk, A.; Szkop, A.; Stachlewska, I. S.; Wang, D.; Reichardt, J.; Skupin, A.; Mattis, I.; Trickl, T.; Vogelmann, H.; Navas-Guzmán, F.; Haefele, A.; Acheson, K.; Ruth, A. A.; Tatarov, B.; Müller, D.; Hu, Q.; Podvin, T.; Goloub, P.; Veselovskii, I.; Pietras, C.; Haeffelin, M.; Fréville, P.; Sicard, M.; Comerón, A.; García, A. J. F.; Menéndez, F. M.; Córdoba-Jabonero, C.; Guerrero-Rascado, J. L.; Alados-Arboledas, L.; Bortoli, D.; Costa, M. J.; Dionisi, D.; Liberti, G. L.; Wang, X.; Sannino, A.; Papagiannopoulos, N.; Boselli, A.; Mona, L.; D'Amico, G.; Romano, S.; Perrone, M. R.; Belegante, L.; Nicolae, D.; Grigorov, I.; Gialitaki, A.; Amiridis, V.; Soupiona, O.; Papayannis, A.; Mamouri, R. E.; Nisantzi, A.; Heese, B.; Hofer, J.; Schechner, Y. Y.; Wandinger, U.; Pappalardo, G. The Unprecedented 2017-2018 Stratospheric Smoke Event: Decay Phase and Aerosol Properties Observed with the EARLINET. *Atmos. Chem. Phys.* **2019**, *19*, 15183−15198.
(24) Schill, G. P.; Froyd, K. D.; Bian, H.; Kupc, A.; Williamson, C.; Brock, C. B.; Ray, E.; Hornbrook, R. S.; Hills, A. J.; Apel, E. C.; Chin, M.; Colarco, P. R.; Murphy, D. M. Widespread Biomass Burning Smoke throughout the Remote Troposphere. *Nat. Geosci.* **2020**, *13*, 422−427.
(25) Wong, J. P. S.; Tsagkaraki, M.; Tsiodra, I.; Mihalopoulos, N.; Violaki, K.; Kanakidou, M.; Sciare, J.; Nenes, A.; Weber, R. J. Effects of Atmospheric Processing on the Oxidative Potential of Biomass Burning Organic Aerosols. *Environ. Sci. Technol.* **2019**, *53*, 6747−6756.
(26) Tuet, W. Y.; Chen, Y.; Fok, S.; Gao, D.; Weber, R. J.; Champion, J. A.; Ng, N. L. Chemical and Cellular Oxidant Production Induced by Naphthalene Secondary Organic Aerosol (SOA): Effect of Redox-Active Metals and Photochemical Aging. *Sci. Rep.* **2017**, *7*, No. 15157.
(27) Zhang, L.; Jaffe, D. A. Trends and Sources of Ozone and Sub-Micron Aerosols at the Mt. Bachelor Observatory (MBO) during 2004−2015. *Atmos. Environ.* **2017**, *165*, 143−154.
(28) Barbero, R.; Abatzoglou, J. T.; Larkin, N. K.; Kolden, C. A.; Stocks, B. Climate Change Presents Increased Potential for Very Large Fires in the Contiguous United States. *Int. J. Wildland Fire* **2015**, *24*, 892−899.
(29) Spracklen, D. V.; Mickley, L. J.; Logan, J. A.; Hudman, R. C.; Yevich, R.; Flannigan, M. D.; Westerling, A. L. Impacts of Climate Change from 2000 to 2050 on Wildfire Activity and Carbonaceous Aerosol Concentrations in the Western United States. *J. Geophys. Res.: Atmos.* **2009**, *114*, No. D20301.
(30) Jimenez, J. L.; Canagaratna, M. R.; Donahue, N. M.; Prevot, A. S. H.; Zhang, Q.; Kroll, J. H.; DeCarlo, P. F.; Allan, J. D.; Coe, H.; Ng, N. L.; Aiken, A. C.; Docherty, K. S.; Ulbrich, I. M.; Grieshop, A. P.; Robinson, A. L.; Duplissy, J.; Smith, J. D.; Wilson, K. R.; Lanz, V. A.; Hueglin, C.; Sun, Y. L.; Tian, J.; Laaksonen, A.; Raatikainen, T.; Rautiainen, J.; Vaattovaara, P.; Ehn, M.; Kulmala, M.; Tomlinson, J. M.; Collins, D. R.; Cubison, M. J.; Dunlea, E. J.; Huffman, J. A.; Onasch, T. B.; Alfarra, M. R.; Williams, P. I.; Bower, K.; Kondo, Y.; Schneider, J.; Drewnick, F.; Borrmann, S.; Weimer, S.; Demerjian, K.; Salcedo, D.; Cottrell, L.; Griffin, R.; Takami, A.; Miyoshi, T.; Hatakeyama, S.; Shimono, A.; Sun, J. Y.; Zhang, Y. M.; Dzepina, K.; Kimmel, J. R.; Sueper, D.; Jayne, J. T.; Herndon, S. C.; Trimborn, A. M.; Williams, L. R.; Wood, E. C.; Middlebrook, A. M.; Kolb, C. E.; Baltensperger, U.; Worsnop, D. R. Evolution of Organic Aerosols in the Atmosphere. *Science* **2009**, *326*, 1525−1529.
(31) Huffman, J. A.; Docherty, K. S.; Mohr, C.; Cubison, M. J.; Ulbrich, I. M.; Ziemann, P. J.; Onasch, T. B.; Jimenez, J. L. Chemically-Resolved Volatility Measurements of Organic Aerosol from Different Sources. *Environ. Sci. Technol.* **2009**, *43*, 5351−5357.
(32) Lim, C. Y.; Hagan, D. H.; Coggon, M. M.; Koss, A. R.; Sekimoto, K.; De Gouw, J.; Warneke, C.; Cappa, C. D.; Kroll, J. H. Secondary Organic Aerosol Formation from the Laboratory Oxidation of Biomass Burning Emissions. *Atmos. Chem. Phys.* **2019**, *19*, 12797−12809.
(33) Donahue, N. M.; Kroll, J. H.; Pandis, S. N.; Robinson, A. L. A Two-Dimensional Volatility Basis Set − Part 2: Diagnostics of Organic-Aerosol Evolution. *Atmos. Chem. Phys.* **2012**, *12*, 615−634.
(34) Palm, B. B.; Peng, Q.; Fredrickson, C. D.; Lee, B. H.; Garofalo, L. A.; Pothier, M. A.; et al. Quantification of Organic Aerosol and Brown Carbon Evolution in Fresh Wildfire Plumes. *Proc. Natl. Acad. Sci. U.S.A.* **2020**, *117*, 29469−29477.
(35) Collier, S.; Zhou, S.; Onasch, T. B.; Jaffe, D. A.; Kleinman, L.; Sedlacek, A. J.; Briggs, N. L.; Hee, J.; Fortner, E.; Shilling, J. E.; Worsnop, D.; Yokelson, R. J.; Parworth, C.; Ge, X.; Xu, J.; Butterfield, Z.; Chand, D.; Dubey, M. K.; Pekour, M. S.; Springston, S.; Zhang, Q. Regional Influence of Aerosol Emissions from Wildfires Driven by Combustion Efficiency: Insights from the BBOP Campaign. *Environ. Sci. Technol.* **2016**, *50*, 8613−8622.
(36) Liu, Y.; Goodrick, S.; Heilman, W. Wildland Fire Emissions, Carbon, and Climate: Wildfire-Climate Interactions. *For. Ecol. Manage.* **2014**, *317*, 80−96.
(37) Cubison, M. J.; Ortega, A. M.; Hayes, P. L.; Farmer, D. K.; Day, D.; Lechner, M. J.; Brune, W. H.; Apel, E.; Diskin, G. S.; Fisher, J. A.; Fuelberg, H. E.; Hecobian, A.; Knapp, D. J.; Mikoviny, T.; Riemer, D.; Sachse, G. W.; Sessions, W.; Weber, R. J.; Weinheimer, A. J.; Wisthaler, A.; Jimenez, J. L. Effects of Aging on Organic Aerosol from Open Biomass Burning Smoke in Aircraft and Laboratory Studies. *Atmos. Chem. Phys.* **2011**, *11*, 12049−12064.
(38) May, A. A.; McMeeking, G. R.; Lee, T.; Taylor, J. W.; Craven, J. S.; Burling, I. R.; Sullivan, A. P.; Akagi, S. K.; Collett, J. L.; Flynn, M. J.; Coe, H.; Urbanski, S. P.; Seinfeld, J. H.; Yokelson, R. J.; Kreidenweis, S. M. Aerosol Emissions from Prescribed Fires in the United States: A Synthesis of Laboratory and Aircraft Measurements. *J. Geophys. Res.: Atmos.* **2014**, *119*, 11826−11849.
(39) Coggon, M. M.; Veres, P. R.; Yuan, B.; Koss, A.; Warneke, C.; Gilman, J. B.; Lerner, B. M.; Peischl, J.; Aikin, K. C.; Stockwell, C. E.; Hatch, L. E.; Ryerson, T. B.; Roberts, J. M.; Yokelson, R. J.; de Gouw, J. A. Emissions of Nitrogen-Containing Organic Compounds from the Burning of Herbaceous and Arboraceous Biomass: Fuel Composition Dependence and the Variability of Commonly Used Nitrile Tracers. *Geophys. Res. Lett.* **2016**, *43*, 9903−9912.
(40) Kleinman, L.; Sedlacek, A., III; Adachi, K.; Buseck, P.; Collier, S.; Dubey, M.; Hodshire, A.; Lewis, E.; Onasch, T.; Pierce, J.; Shilling, J.; Springston, S.; Wang, J.; Zhang, Q.; Zhou, S.; Yokelson, R. Rapid Evolution of Aerosol Particles and Their Optical Properties Downwind of Wildfires in the Western U.S. *Atmos. Chem. Phys.* **2020**, *20*, 13319−13341.
(41) Cappa, C. D.; Lim, C. Y.; Hagan, D. H.; Coggon, M.; Koss, A.; Sekimoto, K.; de Gouw, J.; Onasch, T. B.; Warneke, C.; Kroll, J. H. Biomass-Burning-Derived Particles from a Wide Variety of Fuels: Part 2: Effects of Photochemical Aging on Particle Optical and Chemical Properties. *Atmos. Chem. Phys.* **2020**, *20*, 8511−8532.
(42) Dzepina, K.; Mazzoleni, C.; Fialho, P.; China, S.; Zhang, B.; Owen, R. C.; Helmig, D.; Hueber, J.; Kumar, S.; Perlinger, J. A.; Kramer, L. J.; Dziobak, M. P.; Ampadu, M. T.; Olsen, S.; Wuebbles, D. J.; Mazzoleni, L. R. Molecular Characterization of Free Tropospheric Aerosol Collected at the Pico Mountain Observatory: A Case Study with a Long-Range Transported Biomass Burning Plume. *Atmos. Chem. Phys.* **2015**, *15*, 5047−5068.
(43) Zuidema, P.; Sedlacek, A. J.; Flynn, C.; Springston, S.; Delgadillo, R.; Zhang, J.; Aiken, A. C.; Koontz, A.; Muradyan, P. The Ascension Island Boundary Layer in the Remote Southeast Atlantic Is Often Smoky. *Geophys. Res. Lett.* **2018**, *45*, 4456−4465.

https://doi.org/10.1021/acs.est.1c07301
Environ. Sci. Technol. 2022, 56, 3645−3657

(44) Du, W.; Sun, Y. L.; Xu, Y. S.; Jiang, Q.; Wang, Q. Q.; Yang, W.; Wang, F.; Bai, Z. P.; Zhao, X. D.; Yang, Y. C. Chemical Characterization of Submicron Aerosol and Particle Growth Events at a National Background Site (3295 m a. s. l.) on the Tibetan Plateau. *Atmos. Chem. Phys.* **2015**, *15*, 10811−10824.
(45) Zhang, X.; Xu, J.; Kang, S.; Liu, Y.; Zhang, Q. Chemical Characterization of Long-Range Transport Biomass Burning Emissions to the Himalayas: Insights from High-Resolution Aerosol Mass Spectrometry. *Atmos. Chem. Phys.* **2018**, *18*, 4617−4638.
(46) Wang, J.; Zhang, Q.; Chen, M.; Collier, S.; Zhou, S.; Ge, X.; Xu, J.; Shi, J.; Xie, C.; Hu, J.; Ge, S.; Sun, Y.; Coe, H. First Chemical Characterization of Refractory Black Carbon Aerosols and Associated Coatings over the Tibetan Plateau (4730 m a.s.L). *Environ. Sci. Technol.* **2017**, *51*, 14072−14082.
(47) Schurman, M. I.; Lee, T.; Desyaterik, Y.; Schichtel, B. A.; Kreidenweis, S. M.; Collett, J. L. Transport, Biomass Burning, and in-Situ Formation Contribute to Fine Particle Concentrations at a Remote Site near Grand Teton National Park. *Atmos. Environ.* **2015**, *112*, 257−268.
(48) Weiss-Penzias, P.; Jaffe, D. A.; Swartzendruber, P.; Dennison, J. B.; Chand, D.; Hafner, W.; Prestbo, E. Observations of Asian Air Pollution in the Free Troposphere at Mount Bachelor Observatory during the Spring of 2004. *J. Geophys. Res.: Atmos.* **2006**, *111*, No. D10304.
(49) Reidmiller, D. R.; Jaffe, D. A.; Chandl, D.; Strodel, S.; Swartzendruber, P.; Wolfe, G. M.; Thornton, J. A. Interannual Variability of Long-Range Transport as Seen at the Mt. Bachelor Observatory. *Atmos. Chem. Phys.* **2009**, *9*, 557−572.
(50) Zhou, S.; Collier, S.; Jaffe, D. A.; Zhang, Q. Free Tropospheric Aerosols at the Mt. Bachelor Observatory: More Oxidized and Higher Sulfate Content Compared to Boundary Layer Aerosols. *Atmos. Chem. Phys.* **2019**, *19*, 1571−1585.
(51) Onasch, T. B.; Trimborn, A.; Fortner, E. C.; Jayne, J. T.; Kok, G. L.; Williams, L. R.; Davidovits, P.; Worsnop, D. R. Soot Particle Aerosol Mass Spectrometer: Development, Validation, and Initial Application. *Aerosol Sci. Technol.* **2012**, *46*, 804−817.
(52) Avery, A. M.; Williams, L. R.; Fortner, E. C.; Robinson, W. A.; Onasch, T. B. Particle Detection Using the Dual-Vaporizer Configuration of the Soot Particle Aerosol Mass Spectrometer (SP-AMS). *Aerosol Sci. Technol.* **2021**, *55*, 254−267.
(53) Canagaratna, M. R.; Jayne, J. T.; Jimenez, J. L.; Allan, J. D.; Alfarra, M. R.; Zhang, Q.; Onasch, T. B.; Drewnick, F.; Coe, H.; Middlebrook, A.; Delia, A.; Williams, L. R.; Trimborn, A. M.; Northway, M. J.; DeCarlo, P. F.; Kolb, C. E.; Davidovits, P.; Worsnop, D. R. Chemical and Microphysical Characterization of Ambient Aerosols with the Aerodyne Aerosol Mass Spectrometer. *Mass Spectrom. Rev.* **2007**, *26*, 185−222.
(54) DeCarlo, P. F.; Kimmel, J. R.; Trimborn, A.; Northway, M. J.; Jayne, J. T.; Aiken, A. C.; Gonin, M.; Fuhrer, K.; Horvath, T.; Docherty, K. S.; Worsnop, D. R.; Jimenez, J. L. Field-Deployable, High-Resolution, Time-of-Flight Aerosol Mass Spectrometer. *Anal. Chem.* **2006**, *78*, 8281−8289.
(55) Fierz, M.; Vernooij, M. G. C.; Burtscher, H. An Improved Low-Flow Thermodenuder. *J. Aerosol Sci.* **2007**, *38*, 1163−1168.
(56) Müller, M.; Mikoviny, T.; Feil, S.; Haidacher, S.; Hanel, G.; Hartungen, E.; Jordan, A.; Märk, L.; Mutschlechner, P.; Schottkowsky, R.; Sulzer, P.; Crawford, J. H.; Wisthaler, A. A Compact PTR-ToF-MS Instrument for Airborne Measurements of Volatile Organic Compounds at High Spatiotemporal Resolution. *Atmos. Meas. Tech.* **2014**, *7*, 3763−3772.
(57) Permar, W.; Wang, Q.; Selimovic, V.; Wielgasz, R. J.; Yokelson, R. J.; Hornbrook, R. S.; Hills, A. J.; Apel, E.; Ku, I.; Zhou, Y.; Sive, B. C.; Sullivan, A. P.; Collett, J. L.; Campos, T. L.; Palm, B. B.; Peng, Q.; Thornton, J. A.; Garofalo, L. A.; Farmer, D. K.; Kreidenweis, S. M.; Levin, E. J. T.; DeMott, P. J.; Flocke, F.; Hu, L.; et al. Emissions of Trace Organic Gases from Western U.S. Wildfires Based on WE-CAN Aircraft Measurements. *J. Geophys. Res.: Atmos.* **2021**, *126*, No. e2020JD033838.
(58) Anderson, T. L.; Ogren, J. A. Determining Aerosol Radiative Properties Using the TSI 3563 Integrating Nephelometer. *Aerosol Sci. Technol.* **1998**, *29*, 57−69.
(59) Canagaratna, M. R.; Jimenez, J. L.; Kroll, J. H.; Chen, Q.; Kessler, S. H.; Massoli, P.; Hildebrandt Ruiz, L.; Fortner, E.; Williams, L. R.; Wilson, K. R.; Surratt, J. D.; Donahue, N. M.; Jayne, J. T.; Worsnop, D. R. Elemental Ratio Measurements of Organic Compounds Using Aerosol Mass Spectrometry: Characterization, Improved Calibration, and Implications. *Atmos. Chem. Phys.* **2015**, *15*, 253−272.
(60) Paatero, P.; Tapper, U. Positive Matrix Factorization: A Non-negative Factor Model with Optimal Utilization of Error Estimates of Data Values. *Environmetrics* **1994**, *5*, 111−126.
(61) Ulbrich, I. M.; Canagaratna, M. R.; Zhang, Q.; Worsnop, D. R.; Jimenez, J. L. Interpretation of Organic Components from Positive Matrix Factorization of Aerosol Mass Spectrometric Data. *Atmos. Chem. Phys.* **2009**, *9*, 2891−2918.
(62) Zhang, Q.; Jimenez, J. L.; Canagaratna, M. R.; Ulbrich, I. M.; Ng, N. L.; Worsnop, D. R.; Sun, Y. Understanding Atmospheric Organic Aerosols via Factor Analysis of Aerosol Mass Spectrometry: A Review. *Anal. Bioanal. Chem.* **2011**, *401*, 3045−3067.
(63) Sun, Y. L.; Zhang, Q.; Schwab, J. J.; Yang, T.; Ng, N. L.; Demerjian, K. L. Factor Analysis of Combined Organic and Inorganic Aerosol Mass Spectra from High Resolution Aerosol Mass Spectrometer Measurements. *Atmos. Chem. Phys.* **2012**, *12*, 8537−8551.
(64) Alfarra, M. R.; Prevot, A. S. H.; Szidat, S.; Sandradewi, J.; Weimer, S.; Lanz, V. A.; Schreiber, D.; Mohr, M.; Baltensperger, U. Identification of the Mass Spectral Signature of Organic Aerosols from Wood Burning Emissions. *Environ. Sci. Technol.* **2007**, *41*, 5770−5777.
(65) Schneider, J.; Weimer, S.; Drewnick, F.; Borrmann, S.; Helas, G.; Gwaze, P.; Schmid, O.; Andreae, M. O.; Kirchner, U. Mass Spectrometric Analysis and Aerodynamic Properties of Various Types of Combustion-Related Aerosol Particles. *Int. J. Mass Spectrom.* **2006**, *258*, 37−49.
(66) Aiken, A. C.; De Foy, B.; Wiedinmyer, C.; Decarlo, P. F.; Ulbrich, I. M.; Wehrli, M. N.; Szidat, S.; Prevot, A. S. H.; Noda, J.; Wacker, L.; Volkamer, R.; Fortner, E.; Wang, J.; Laskin, A.; Shutthanandan, V.; Zheng, J.; Zhang, R.; Paredes-Miranda, G.; Arnott, W. P.; Molina, L. T.; Sosa, G.; Querol, X.; Jimenez, J. L. Mexico City Aerosol Analysis during MILAGRO Using High Resolution Aerosol Mass Spectrometry at the Urban Supersite (T0)-Part 2: Analysis of the Biomass Burning Contribution and the Non-Fossil Carbon Fraction. *Atmos. Chem. Phys.* **2010**, *10*, 5315−5341.
(67) Müller, M.; Anderson, B. E.; Beyersdorf, A. J.; Crawford, J. H.; Diskin, G. S.; Eichler, P.; Fried, A.; Keutsch, F. N.; Mikoviny, T.; Thornhill, K. L.; Walega, J. G.; Weinheimer, A. J.; Yang, M.; Yokelson, R. J.; Wisthaler, A. In Situ Measurements and Modeling of Reactive Trace Gases in a Small Biomass Burning Plume. *Atmos. Chem. Phys.* **2016**, *16*, 3813−3824.
(68) Forrister, H.; Liu, J.; Scheuer, E.; Dibb, J.; Ziemba, L.; Thornhill, K. L.; Anderson, B.; Diskin, G.; Perring, A. E.; Schwarz, J. P.; Campuzano-Jost, P.; Day, D. A.; Palm, B. B.; Jimenez, J. L.; Nenes, A.; Weber, R. J. Evolution of Brown Carbon in Wildfire Plumes. *Geophys. Res. Lett.* **2015**, *42*, 4623−4630.
(69) Ng, N. L.; Canagaratna, M. R.; Zhang, Q.; Jimenez, J. L.; Tian, J.; Ulbrich, I. M.; Kroll, J. H.; Docherty, K. S.; Chhabra, P. S.; Bahreini, R.; Murphy, S. M.; Seinfeld, J. H.; Hildebrandt, L.; Donahue, N. M.; Decarlo, P. F.; Lanz, V. A.; Prévôt, A. S. H.; Dinar, E.; Rudich, Y.; Worsnop, D. R. Organic Aerosol Components Observed in Northern Hemispheric Datasets from Aerosol Mass Spectrometry. *Atmos. Chem. Phys.* **2010**, *10*, 4625−4641.
(70) Ortega, A. M.; Day, D. A.; Cubison, M. J.; Brune, W. H.; Bon, D.; De Gouw, J. A.; Jimenez, J. L. Secondary Organic Aerosol Formation and Primary Organic Aerosol Oxidation from Biomass-Burning Smoke in a Flow Reactor during FLAME-3. *Atmos. Chem. Phys.* **2013**, *13*, 11551−11571.

https://doi.org/10.1021/acs.est.1c07301
Environ. Sci. Technol. 2022, 56, 3645−3657

(71) Andreae, M. O. Soot Carbon and Excess Fine Potassium: Long-Range Transport of Combustion-Derived Aerosols. *Science* **1983**, *220*, 1148−1151.
(72) Park, R. J.; Jacob, D. J.; Logan, J. A. Fire and Biofuel Contributions to Annual Mean Aerosol Mass Concentrations in the United States. *Atmos. Environ.* **2007**, *41*, 7389−7400.
(73) Ma, Y.; Weber, R. J.; Lee, Y. N.; Orsini, D. A.; Maxwell-Meier, K.; Thornton, D. C.; Bandy, A. R.; Clarke, A. D.; Blake, D. R.; Sachse, G. W.; Fuelberg, H. E.; Kiley, C. M.; Woo, J. H.; Streets, D. G.; Carmichael, G. R. Characteristics and Influence of Biosmoke on the Fine-Particle Ionic Composition Measured in Asian Outflow during the Transport and Chemical Evolution over the Pacific (TRACE-P) Experiment. *J. Geophys. Res.: Atmos.* **2003**, *108*, No. 8816.
(74) Drewnick, F.; Diesch, J. M.; Faber, P.; Borrmann, S. Aerosol Mass Spectrometry: Particle-Vaporizer Interactions and Their Consequences for the Measurements. *Atmos. Meas. Tech.* **2015**, *8*, 3811−3830.
(75) Lee, A. K. Y.; Willis, M. D.; Healy, R. M.; Wang, J. M.; Jeong, C. H.; Wenger, J. C.; Evans, G. J.; Abbatt, J. P. D. Single-Particle Characterization of Biomass Burning Organic Aerosol (BBOA): Evidence for Non-Uniform Mixing of High Molecular Weight Organics and Potassium. *Atmos. Chem. Phys.* **2016**, *16*, 5561−5572.
(76) Maudlin, L. C.; Wang, Z.; Jonsson, H. H.; Sorooshian, A. Impact of Wildfires on Size-Resolved Aerosol Composition at a Coastal California Site. *Atmos. Environ.* **2015**, *119*, 59−68.
(77) Chen, L. A.; Moosmüller, H.; Arnott, W. P.; Chow, J. C.; Watson, J. G.; Susott, R. A.; Babbitt, R. E.; Wold, C. E.; Lincoln, E. N.; Wei, M. H. Emissions from Laboratory Combustion of Wildland Fuels: Emission Factors and Source Profiles. *Environ. Sci. Technol.* **2007**, *41*, 4317−4325.
(78) Martin, M. V.; Logan, J. A.; Kahn, R. A.; Leung, F.; Nelson, D. L.; Diner, D. J. Smoke Injection Heights from Fires in North America: Analysis of 5 Years of Satellite Observations. *Atmos. Chem. Phys.* **2010**, *10*, 1491−1510.
(79) Setyan, A.; Zhang, Q.; Merkel, M.; Knighton, W. B.; Sun, Y.; Song, C.; Shilling, J. E.; Onasch, T. B.; Herndon, S. C.; Worsnop, D. R.; Fast, J. D.; Zaveri, R. A.; Berg, L. K.; Wiedensohler, A.; Flowers, B. A.; Dubey, M. K.; Subramanian, R. Characterization of Submicron Particles Influenced by Mixed Biogenic and Anthropogenic Emissions Using High-Resolution Aerosol Mass Spectrometry: Results from CARES. *Atmos. Chem. Phys.* **2012**, *12*, 8131−8156.
(80) Kiendler-Scharr, A.; Zhang, Q.; Hohaus, T.; Kleist, E.; Mensah, A.; Mentel, T. F.; Spindler, C.; Uerlings, R.; Tillmann, R.; Wildt, J. Aerosol Mass Spectrometric Features of Biogenic SOA: Observations from a Plant Chamber and in Rural Atmospheric Environments. *Environ. Sci. Technol.* **2009**, *43*, 8166−8172.
(81) Baylon, P.; Jaffe, D. A.; Wigder, N. L.; Gao, H.; Hee, J. Ozone Enhancement in Western US Wildfire Plumes at the Mt. Bachelor Observatory: The Role of NOx. *Atmos. Environ.* **2015**, *109*, 297−304.
(82) de Gouw, J. A.; Warneke, C.; Parrish, D. D.; Holloway, J. S.; Trainer, M.; Fehsenfeld, F. C. Emission Sources and Ocean Uptake of Acetonitrile (CH 3 CN) in the Atmosphere. *J. Geophys. Res.: Atmos.* **2003**, *108*, No. 4329.
(83) Jiang, J.; Carter, W. P. L.; Cocker, D. R.; Barsanti, K. C. Development and Evaluation of a Detailed Mechanism for Gas-Phase Atmospheric Reactions of Furans. *ACS Earth Space Chem.* **2020**, *4*, 1254−1268.
(84) Roberts, J.; Stockwell, C.; Yokelson, R.; de Gouw, J.; Liu, Y.; Selimovic, V.; Koss, A.; Sekimoto, K.; Coggon, M.; Yuan, B.; Zarzana, K.; Brown, S.; Santin, C.; Doerr, S.; Warneke, C. The Nitrogen Budget of Laboratory-Simulated Western U.S. Wildfires during the FIREX 2016 FireLab Study. *Atmos. Chem. Phys.* **2020**, *20*, 8807−8826.
(85) Chen, L. A.; Verburg, P.; Shackelford, A.; Zhu, D.; Susfalk, R.; Chow, J. C.; Watson, J. G. Moisture Effects on Carbon and Nitrogen Emission from Burning of Wildland Biomass. *Atmos. Chem. Phys.* **2010**, *10*, 6617−6625.
(86) Kondo, Y.; Matsui, H.; Moteki, N.; Sahu, L.; Takegawa, N.; Kajino, M.; Zhao, Y.; Cubison, M. J.; Jimenez, J. L.; Vay, S.; Diskin, G. S.; Anderson, B.; Wisthaler, A.; Mikoviny, T.; Fuelberg, H. E.; Blake, D. R.; Huey, G.; Weinheimer, A. J.; Knapp, D. J.; Brune, W. H. Emissions of Black Carbon, Organic, and Inorganic Aerosols from Biomass Burning in North America and Asia in 2008. *J. Geophys. Res.: Atmos.* **2011**, *116*, No. D08204.
(87) Pan, X.; Kanaya, Y.; Taketani, F.; Miyakawa, T.; Inomata, S.; Komazaki, Y.; Tanimoto, H.; Wang, Z.; Uno, I.; Wang, Z. Emission Characteristics of Refractory Black Carbon Aerosols from Fresh Biomass Burning: A Perspective from Laboratory Experiments. *Atmos. Chem. Phys.* **2017**, *17*, 13001−13016.
(88) Selimovic, V.; Yokelson, R. J.; McMeeking, G. R.; Coefield, S. In-Situ Measurements of Trace Gases, PM, and Aerosol Optical Properties during the 2017 NW US Wildfire Smoke Event. *Atmos. Chem. Phys. Discuss.* **2018**, 1−37.
(89) Grieshop, A. P.; Logue, J. M.; Donahue, N. M.; Robinson, A. L. Laboratory Investigation of Photochemical Oxidation of Organic Aerosol from Wood Fires 1: Measurement and Simulation of Organic Aerosol Evolution. *Atmos. Chem. Phys.* **2009**, *9*, 1263−1277.
(90) Zauscher, M. D.; Wang, Y.; Moore, M. J. K.; Gaston, C. J.; Prather, K. A. Air Quality Impact and Physicochemical Aging of Biomass Burning Aerosols during the 2007 San Diego Wildfires. *Environ. Sci. Technol.* **2013**, *47*, 7633−7643.
(91) Young, D. E.; Kim, H.; Parworth, C.; Zhou, S.; Zhang, X.; Cappa, C. D.; Seco, R.; Kim, S.; Zhang, Q. Influences of Emission Sources and Meteorology on Aerosol Chemistry in a Polluted Urban Environment: Results from DISCOVER-AQ California. *Atmos. Chem. Phys.* **2016**, *16*, 5427−5451.
(92) Ge, X.; Setyan, A.; Sun, Y.; Zhang, Q. Primary and Secondary Organic Aerosols in Fresno, California during Wintertime: Results from High Resolution Aerosol Mass Spectrometry. *J. Geophys. Res.: Atmos.* **2012**, *117*, No. D19301.
(93) Laing, J. R.; Jaffe, D. A.; Hee, J. R. Physical and Optical Properties of Aged Biomass Burning Aerosol from Wildfires in Siberia and the Western USA at the Mt. Bachelor Observatory. *Atmos. Chem. Phys.* **2016**, *16*, 15185−15197.
(94) Jolleys, M. D.; Coe, H.; McFiggans, G.; Capes, G.; Allan, J. D.; Crosier, J.; Williams, P. I.; Allen, G.; Bower, K. N.; Jimenez, J. L.; Russell, L. M.; Grutter, M.; Baumgardner, D. Characterizing the Aging of Biomass Burning Organic Aerosol by Use of Mixing Ratios: A Meta-Analysis of Four Regions. *Environ. Sci. Technol.* **2012**, *46*, 13093−13102.
(95) Yokelson, R. J.; Crounse, J. D.; DeCarlo, P. F.; Karl, T.; Urbanski, S.; Atlas, E.; Campos, T.; Shinozuka, Y.; Kapustin, V.; Clarke, A. D.; Weinheimer, A.; Knapp, D. J.; Montzka, D. D.; Holloway, J.; Weibring, P.; Flocke, F.; Zheng, W.; Toohey, D.; Wennberg, P. O.; Wiedinmyer, C.; Mauldin, L.; Fried, A.; Richter, D.; Walega, J.; Jimenez, J. L.; Adachi, K.; Buseck, P. R.; Hall, S. R.; Shetter, R. Emissions from Biomass Burning in the Yucatan. *Atmos. Chem. Phys.* **2009**, *9*, 5785−5812.
(96) Garofalo, L. A.; Pothier, M. A.; Levin, E. J. T.; Campos, T.; Kreidenweis, S. M.; Farmer, D. K. Emission and Evolution of Submicron Organic Aerosol in Smoke from Wildfires in the Western United States. *ACS Earth Space Chem.* **2019**, *3*, 1237−1247.
(97) Akagi, S. K.; Craven, J. S.; Taylor, J. W.; McMeeking, G. R.; Yokelson, R. J.; Burling, I. R.; Urbanski, S. P.; Wold, C. E.; Seinfeld, J. H.; Coe, H.; Alvarado, M. J.; Weise, D. R. Evolution of Trace Gases and Particles Emitted by a Chaparral Fire in California. *Atmos. Chem. Phys.* **2012**, *12*, 1397−1421.
(98) Jolleys, M.; Coe, H.; McFiggans, G.; McMeeking, G. R.; Lee, T.; Kreidenweis, S. M.; Collett, J. L.; Sullivan, A. Organic Aerosol Emission Ratios from the Laboratory Combustion of Biomass Fuels. *J. Geophys. Res.: Atmos.* **2014**, *119*, 12850−12871.

https://doi.org/10.1021/acs.est.1c07301
Environ. Sci. Technol. 2022, 56, 3645−3657